

# Probing renal blood volume with magnetic resonance imaging

Thoralf Niendorf<sup>1</sup>  | Erdmann Seeliger<sup>2</sup> | Kathleen Cantow<sup>2</sup> | Bert Flemming<sup>2</sup> |  
Sonia Waiczies<sup>1</sup>  | Andreas Pohlmann<sup>1</sup> 

<sup>1</sup>Berlin Ultrahigh Field Facility (B.U.F.F.), Max Delbrück Center for Molecular Medicine in the Helmholtz Association, Berlin, Germany

<sup>2</sup>Institute of Physiology, Charité – Universitätsmedizin Berlin, Campus Mitte, and Center for Cardiovascular Research (CCR), Berlin, Germany

## Correspondence

Thoralf Niendorf, Berlin Ultrahigh Field Facility (B.U.F.F.), Max Delbrück Center for Molecular Medicine in the Helmholtz Association, Berlin, Germany.  
Email: thoralf.niendorf@mdc-berlin.de

## Funding information

German Federal Ministry of Education and Research, Grant/Award Number: renalMRoxy, program VIP+, 03VP00081; Deutsche Forschungsgemeinschaft, Grant/Award Number: 394046635

## Abstract

Damage to the kidney substantially reduces life expectancy. Renal tissue hypoperfusion and hypoxia are key elements in the pathophysiology of acute kidney injury and its progression to chronic kidney disease. In vivo assessment of renal haemodynamics and tissue oxygenation remains a challenge. Blood oxygenation level-dependent (BOLD) magnetic resonance imaging (MRI) is sensitive to changes in the effective transversal relaxation time ( $T_2^*$ ) in vivo, and is non-invasive and indicative of renal tissue oxygenation. However, the renal  $T_2^*$  to tissue  $pO_2$  relationship is not governed exclusively by renal blood oxygenation, but is affected by physiological confounders with alterations in renal blood volume fraction (BVf) being of particular relevance. To decipher this interference probing renal BVf is essential for the pursuit of renal MR oximetry. Superparamagnetic iron oxide nanoparticle (USPIO) preparations can be used as MRI visible blood pool markers for detailing alterations in BVf. This review promotes the opportunities of MRI-based assessment of renal BVf. Following an outline on the specifics of renal oxygenation and perfusion, changes in renal BVf upon interventions and their potential impact on renal  $T_2^*$  are discussed. We also describe the basic principles of renal BVf assessment using ferumoxytol-enhanced MRI in the equilibrium concentration regimen. We demonstrate that ferumoxytol does not alter control of renal haemodynamics and oxygenation. Preclinical applications of ferumoxytol enhanced renal MRI as well as considerations for its clinical implementation for examining renal BVf changes are provided alongside practical considerations. Finally, we explore the future directions of MRI-based assessment of renal BVf.

## KEYWORDS

acute kidney injury, ferumoxytol, magnetic resonance imaging, MR oximetry, renal blood volume fraction, renal oxygenation

## 1 | INTRODUCTION

Kidney diseases pose a global health burden with their steadily increasing incidence.<sup>1–5</sup> Elucidating the efficacy of renoprotective strategies is essential *en route* to novel treatment options and effective prophylactic regimens for acute

kidney injury (AKI) and chronic kidney diseases (CKD).<sup>6</sup> Current AKI and CKD therapies and prevention strategies are largely experience driven.<sup>7</sup> Today's options for targeted and stratified measures are disappointingly sparse.<sup>8</sup> Translational approaches—although urgently warranted—are scarce. One major obstacle is the technology required to non-invasively

This is an open access article under the terms of the Creative Commons Attribution NonCommercial License, which permits use, distribution and reproduction in any medium, provided the original work is properly cited and is not used for commercial purposes.

© 2019 The Authors. *Acta Physiologica* published by John Wiley & Sons Ltd on behalf of Scandinavian Physiological Society

disentangle the pathophysiological complexity of AKI and its progression to CKD. Closing this gap asks for approaches, which are clinically applicable, ubiquitous and non-invasive—the forte of MRI.<sup>9</sup> MRI affords longitudinal studies, high anatomic detail, full kidney coverage, soft tissue contrast that helps to capture the physiological heterogeneity between and within the renal layers, and temporal resolution ranging from seconds to minutes.<sup>9</sup>

Renal tissue hypoperfusion and hypoxia play a prominent role in the early pathophysiology of AKI and probably also promote its progression to CKD.<sup>10–16</sup> Hypoxia results from an imbalance between oxygen ( $O_2$ ) delivery and  $O_2$  consumption.<sup>11,14,17–23</sup> Insights into renal oxygenation can be derived from blood oxygenation level–dependent (BOLD) MRI, which offers a non-invasive in vivo technique.<sup>24</sup> Renal BOLD-MRI methodology has progressed and a large body of literature on (pre)clinical applications<sup>25–31</sup> is available. The growing number of reports eloquently speaking about renal BOLD-MRI and the consensus papers on technical recommendations<sup>32</sup> document the value of non-invasive MRI to renal (patho)physiology. In BOLD MRI image contrast is sensitive to bulk microscopic magnetic field perturbations, which are caused by paramagnetic deoxygenated haemoglobin (deoxyHb) and impact the effective transversal MR relaxation time  $T_2^*$ .<sup>33</sup>  $T_2^*$  weighted MRI is sensitive to changes in the amount of deoxyHb per tissue volume element (voxel).<sup>34</sup>  $T_2^*$  decreases if the volume fraction of deoxyHb increases. Renal  $T_2^*$  or its reciprocal value ( $R_2^*=1/T_2^*$ ) is a surrogate of renal blood oxygenation, but is frequently interpreted also

as a surrogate of renal tissue oxygenation. This assumption is based upon the  $T_2^*$  dependence on  $O_2$  saturation of Hb ( $StO_2$ ), the physiological relationships between  $StO_2$  and blood partial pressure of  $O_2$  ( $pO_2$ ), and between blood  $pO_2$  and tissue  $pO_2$ . Mapping of  $T_2^*$  or of  $R_2^*$  has been employed for the assessment of renal oxygenation in a broad spectrum of renal tissue states and interventions in human and animal studies.<sup>29,35</sup> Renal  $T_2^*$  has even been suggested to display a close correlation with renal tissue  $pO_2$  levels.<sup>36</sup>

Notwithstanding the encouraging progress made, questions have been raised regarding the correct interpretation of BOLD MRI data in the kidney as a surrogate of tissue oxygenation. These questions spurred the debate on “how bold is BOLD-MRI of the kidney?”.<sup>24</sup> This debate was triggered by experimental observations derived from simultaneous measurements of renal  $T_2^*$  and tissue  $pO_2$  using an integrated approach of MRI and gold standard physiological measurements (MR-PHYSIOL).<sup>37–39</sup> MR-PHYSIOL experiments revealed substantial discrepancies in the quantitative relationship between changes in renal  $T_2^*$  and those in renal tissue  $pO_2$  for the different layers of the kidney (cortex, outer medulla, inner medulla) and for various (patho)physiologically relevant interventions to the kidney.<sup>38</sup> In essence, the integrated MR-PHYSIOL approach confirmed that the renal  $T_2^*$  to tissue  $pO_2$  relationship is not governed exclusively by renal blood oxygenation, but is also heavily influenced by a number of physiological confounders as illustrated in Figure 1.

Of particular relevance are alterations in renal blood volume fraction (BFv). As renal  $T_2^*$  is a surrogate for the amount

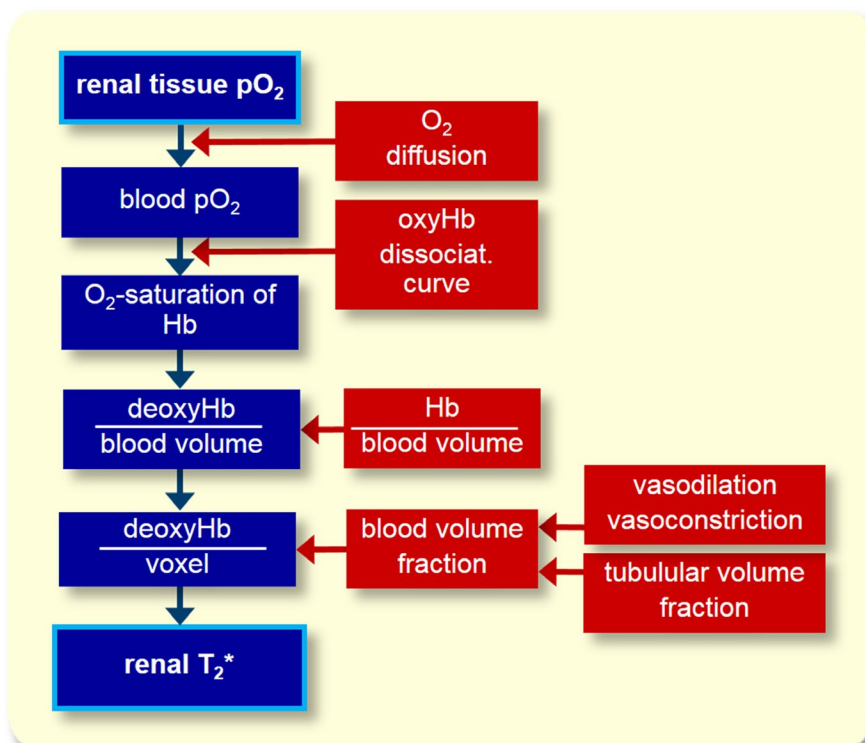


**FIGURE 1** Schematic overview of the relationship between tissue partial pressure of oxygen ( $pO_2$ ) and renal  $T_2^*$ , together with the confounding key factors. This includes  $T_2^*$  alterations as a result of changes in the tubular compartment and/or in the intrarenal vascular compartment. Changes in the renal blood volume fraction induced by either active vasomotion or passive circular vessel distension/compression alter the amount of deoxyHb per tissue volume and may confound  $T_2^*$ . As the renal capsule has a rather low elasticity, changes in tubular volume fraction will often result in circular distension or compression of intrarenal vessels, which will inevitably induce changes in the renal blood volume fraction which may confound  $T_2^*$

of deoxyHb per tissue volume, any change in BVf confounds the interpretation of  $T_2^*$  changes commonly exclusively attributed to alterations in blood oxygenation, and even more so as tissue oxygenation. This confounding role of BVf has not received careful consideration and assessment so far, although it was recently outlined in reports on alterations in renal vascular conductance, local haemoglobin concentrations and kidney size triggered by physiological interventions.<sup>40</sup> The impact of renal BVf changes on  $T_2^*$  exceeds that of most other organs as a result of the substantial and readily alterable blood volume fraction in the renal cortex.<sup>41</sup> Taking this into account,  $T_2^*$  mapping alone cannot provide an unambiguous examination of renal oxygenation. However, if an assessment of renal BVf is integrated into a comprehensive MR imaging protocol, the combination of renal  $T_2^*$  and BVf mapping could provide a more quantitative surrogate of renal blood oxygenation *en route* to MR oximetry tailored for the in vivo and non-invasive characterization of renal tissue oxygenation and haemodynamics.<sup>24,42</sup>

Realizing the opportunities, challenges and caveats of assessing renal haemodynamics and tissue oxygenation in vivo and non-invasively, probing renal BVf is highly relevant if not essential for the pursuit of renal MR oximetry.<sup>42</sup> Intravenously applied superparamagnetic iron oxide nanoparticle (USPIO) preparations can be used as MRI visible blood pool markers for probing alterations in BVf, in particular ferumoxytol, which is increasingly used off-label as an intravascular MRI contrast agent.<sup>42-47</sup> To promote these advancements at the interface between physics, physiology and patient care, this review discusses the opportunities of ferumoxytol-enhanced assessment of renal BVf. For this purpose, the specifics of renal oxygenation and perfusion are outlined first. Secondly, alterations in renal BVf upon interventions and their impact on  $T_2^*$  are surveyed. The basic physical and biophysical principles of probing BVf using ferumoxytol as a blood pool marker are then described. Next, acute effects of ferumoxytol on controlling renal haemodynamics and oxygenation are considered. Preclinical applications of ferumoxytol-enhanced MRI are presented for monitoring of renal BVf in physiological settings where significant variations in both, renal BVf and oxygenation, occur. Considerations for clinical implementation of ferumoxytol-based assessment of renal BVf changes are provided. We conclude by exploring future directions of MRI-based assessment of renal BVf.

All the animal experiments performed by the authors and shown in the figures were carried out in accordance with published guidelines.<sup>48,49</sup>

## 2 | SPECIFICS OF RENAL PERFUSION AND OXYGENATION

Renal haemodynamics and oxygenation offer a number of striking differences when compared with non-renal

tissue.<sup>24,38</sup> First, total renal blood flow (RBF) is huge when compared with virtually all other organs: the kidneys receive about 20% of the cardiac output under resting conditions. Accordingly, the kidneys' oxygen extraction (the difference between the  $O_2$  content in the renal arterial and the renal venous blood) is low. Yet blood perfusion within the kidneys is quite heterogeneous: while 100% reaches the cortex, only 15% of blood that previously passes through the cortex will reach the medulla. This unequal distribution is one reason behind the very low  $pO_2$  in the medulla. Secondly, the kidney differs from all other organs with regard to the relationship between metabolism and perfusion. More than 26 thousand millimoles of sodium ( $Na^+$ ) are filtered in the human glomeruli every day: this is equivalent to more than 1.5 kg of table salt. To achieve sodium balance, the amount of salt excreted via the urine must exactly match the amount of ingested salt minus that amount of extrarenal loss. Thus, more than 99% of the filtered sodium must usually be reabsorbed from the tubules. Tubular resorption relies on active transport processes, which account for about 90% of the kidney's energy expenditure, and, thus, its  $O_2$  consumption. The more  $Na^+$  is filtered in the glomeruli, the more must be reabsorbed. As glomerular filtration rate (GFR), in general, increases with increased renal blood flow, renal  $O_2$  consumption also usually increases with increased renal perfusion. This is in contrast to all other organs, where metabolism determines perfusion. However, the kidney is equipped with efficient mechanisms of autoregulation, that is, the ability to maintain RBF and GFR relatively constant in the face of changes in renal artery pressure. Renal autoregulation is suggested to serve the purpose of balancing  $O_2$  delivery, that is, RBF, with the metabolic needs and  $O_2$  demands arising from tubular reabsorption.

In addition to the heterogeneous intrarenal blood perfusion, other factors substantially contribute to the low tissue  $pO_2$  and, in particular, the physiological hypoxia in the medulla as summarized in a recent review.<sup>24</sup> First, there is a considerable shunt diffusion of  $O_2$  from arteries to veins in the cortex and from descending to ascending vasa recta in the medulla. Second, the Fahraeus-Lindqvist effect reduces the haematocrit in the vasa recta supplying the medulla, which results in a reduction in the  $O_2$  content of blood perfusing the medulla. Third, plasma skimming at intrarenal vessel branches induces different haematocrit and  $O_2$  content of blood perfusing the daughter vessels.

## 3 | ALTERATIONS IN RENAL BVF UPON INTERVENTIONS AND THEIR IMPACT ON $T_2^*$

Changes in renal BVf, that is, in vessel volume per tissue volume, induced by either active vasomotion or passive circular

vessel distension/compression alter the amount of deoxyHb per tissue volume and thus confound the renal  $T_2^*$  to tissue  $pO_2$  relationship (see Figure 1).<sup>50</sup> If considered per tissue weight, total renal blood flow is much higher than that of most other tissues. It is to be expected that renal vasomotion, at least of cortical vessels, results in renal BVf changes that exceed those documented for other tissues.<sup>10,21,32,35</sup> Substantial changes in the renal BVf were observed for various experimental settings.<sup>7,11,20</sup> Moreover, the tubules are a unique feature of the kidney. Their volume fraction is quite large and can rapidly change as a result of changes in glomerular filtration, alterations in tubular outflow towards the pelvis, changes in tubular fluid resorption and modulation of the transmural pressure gradient. As the renal capsule has a rather low elasticity, changes in tubular volume fraction should often result in circular distension or compression of intrarenal vessels, which will inevitably change the renal BVf.<sup>10</sup>

Figure 1 provides a schematic overview of the confounders of the renal  $T_2^*$  to tissue  $pO_2$  relationship as derived from various studies, in particular studies that assessed the impact of alterations in renal haemodynamics, renal blood and tissue oxygenation, haematocrit, and tubular and vascular volume fractions on  $T_2^*$  under various (patho)physiological conditions.<sup>24</sup> The confounders include (i) changes in  $O_2$  diffusion between blood and tissue, (ii) shifts of the oxyHb dissociation curve, (iii) alterations in Hb concentration per blood volume (haematocrit), (iv) changes in the tubular compartment and (v) changes in the intrarenal vascular compartment (blood volume fraction, BVf). The impact of changes in BVf was demonstrated in pre-clinical studies that revealed suprarenal aortic occlusion (or that of the renal artery) induces only a minor decrease in renal  $T_2^*$ , in contrast to a massive  $T_2^*$  decrease upon occlusion of the renal vein.<sup>24</sup> Simultaneous occlusion of the renal vein and artery yielded an intermediate  $T_2^*$  decrease.<sup>24</sup> In each of these three cases, tissue  $pO_2$ , blood  $pO_2$  and  $StO_2$  approach zero. Yet the BVf is decreased in case of arterial occlusion, augmented for venous occlusion and remains approximately unchanged during common arterio-venous occlusion. Contrary to vasoconstriction, vasodilation induces  $T_2^*$  shortening governed by a BVf increase, although renal tissue  $pO_2$ , blood  $pO_2$ , and  $StO_2$  primarily increase owing to improved  $O_2$  delivery. Vasoconstriction causes a  $T_2^*$  prolongation despite a decline in  $O_2$  delivery as a result of a reduced BVf. Distension of tubules results in increased  $T_2^*$  in the face of primarily unchanged  $StO_2$ , blood and tissue  $pO_2$  caused by reduced BVf.<sup>24</sup> Anaemia or an increase in plasma skimming evoke an increase in  $T_2^*$  despite the drop in  $O_2$  delivery and tissue  $pO_2$ . Finally, alterations in the inspiratory  $O_2$  fraction ( $FiO_2$ ) change renal  $T_2^*$ . Hypoxia decreases  $T_2^*$  in parallel with  $StO_2$ , blood and tissue  $pO_2$ . Changes in BVf may either enhance or diminish this effect on  $T_2^*$ , depending on whether the  $FiO_2$  falls moderately or severely below 21%, leading either to intrarenal vasodilation or vasoconstriction respectively. The effect of hyperoxia on  $T_2^*$  is much less pronounced.

## 4 | BASIC PRINCIPLES OF RENAL BVF ASSESSMENT USING FERUMOXYTOL IN AN EQUILIBRIUM CONCENTRATION REGIMEN

Ferumoxytol-enhanced MRI is susceptible to bulk microscopic magnetic field perturbations around blood vessels, which are induced by the USPIO nanoparticles. These microscopic magnetic field inhomogeneities affect the (effective) transversal MR relaxation times  $T_2^*$  and  $T_2$  as a function of the USPIO concentration.  $T_2^*$  is governed by  $1/T_2^* = 1/T_2 + 1/T_2'$ , with  $T_2$  being the tissue-dependent transverse relaxation time observed in spin-echo MR measurements and  $T_2'$  embodying susceptibility-related contributions.<sup>51</sup> While the magnetic field perturbations caused by Fe atoms (in deoxyHb or USPIO nanoparticles) directly reduce  $T_2^*$ , diffusion effects in the proximity of blood vessels also lead to a decrease in  $T_2$ . When the USPIO concentration increases, a  $T_2^*/T_2$  decrease occurs and hence a signal attenuation in  $T_2^*$ -weighted and  $T_2$ -weighted MR images. Parametric mapping provides quantitative data of the relaxation times  $T_2^*$  and  $T_2$ . Renal  $T_2^*$  maps are commonly obtained with multi-echo gradient echo techniques. With this approach a train of gradient refocused echoes is acquired after the initial excitation, whereby each echo is independently  $T_2^*$  weighted. In vivo  $T_2^*$  mapping of the kidney permits high anatomical detail employing an in-plane spatial resolution as good as 50-100  $\mu m$  in mice and about 250  $\mu m$  in rats with dedicated small animal MR systems equipped with state-of-the-art radiofrequency antenna technology<sup>52</sup> (Figure 2). Parametric mapping of the reciprocal value of renal  $T_2^*$  ( $R_2^* = 1/T_2^*$ ) is used for renal BVf mapping in an equilibrium concentration regimen. For this purpose, renal BVf can be calculated by comparing pre-ferumoxytol data ( $R_2^*$ -maps) with post-ferumoxytol data ( $R_{2,USPIO}^*$  maps).<sup>53</sup>

$$BVf = \frac{3}{4\pi} \cdot \frac{(R_{2,USPIO}^* - R_2^*)}{\Delta\chi_{USPIO} \cdot B_0 \cdot \gamma} = \frac{3}{4\pi} \cdot \frac{\Delta R_{2,USPIO}^*}{\Delta\chi_{USPIO} \cdot B_0 \cdot \gamma} \quad (1)$$

where  $\gamma$  is the gyromagnetic ratio, which is  $2.675 \cdot 10^8$  rad/(s T),  $B_0 = 9.4$  T and  $\Delta\chi_{USPIO}$  is the susceptibility difference between blood with and without added USPIO:  $\Delta\chi_{USPIO} = 0.024$  ppm (cgs units)  $\times$  [USPIO dose in mg Fe/kg body weight].<sup>54</sup> The equilibrium concentration regimen facilitates the monitoring of renal BVf over several hours, supported by the long half-life time of ferumoxytol.<sup>55</sup> Assuming that the magnetic field inhomogeneity is negligible and constant throughout the experiment so that  $R_2^*$  is governed by microscopic rather than by macroscopic susceptibility gradients, renal  $StO_2$  can be estimated using a multi-parametric

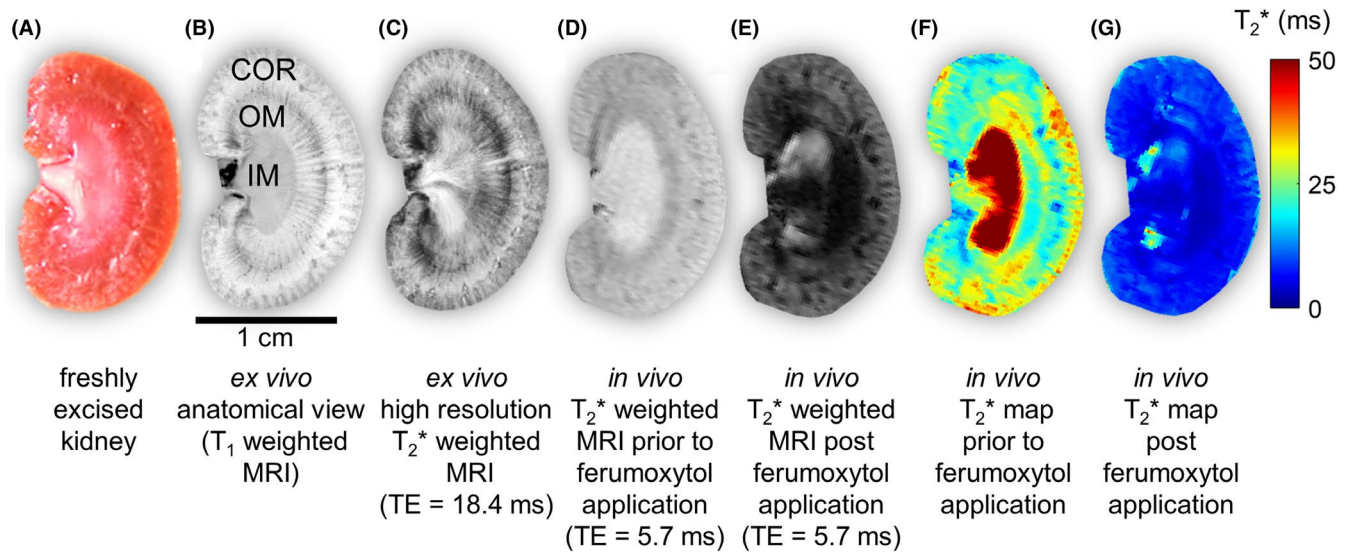


**FIGURE 2** Coronal views of rat kidneys: (A) photograph of a freshly excised rat kidney, (B) T<sub>1</sub>-weighted anatomical MR image acquired *ex vivo* using an in-plane spatial resolution of 50 μm (cortex COR; outer medulla OM; inner medulla IM, the 1 cm scale bar illustrates the size of the rat kidney), (C) T<sub>2</sub>\*-sensitized MR image acquired *ex vivo* using an in-plane spatial resolution 50 μm, (D) T<sub>2</sub>\*-weighted *in vivo* MR image acquired with an in-plane spatial resolution of 300 μm prior to ferumoxytol application, (E) T<sub>2</sub>\*-weighted *in vivo* MR image acquired with an in-plane spatial resolution of 300 μm after ferumoxytol application, (F) *in vivo* T<sub>2</sub>\* map acquired at baseline with an in-plane spatial resolution of 300 μm and (G) *in vivo* T<sub>2</sub>\* map acquired post-ferumoxytol administration with an in-plane spatial resolution of 300 μm. The T<sub>2</sub>\* shortening caused by the superparamagnetic effect of ferumoxytol can be readily recognized

MR approach including renal R<sub>2</sub><sup>\*</sup>, R<sub>2</sub> and BVf and a solution of the model equation  $s(t) = f(t, BVf, SO_2, \dots)$  for  $StO_2 = f(R_2^*, R_2, BVf, \dots)$ <sup>56-58</sup>:

$$StO_2 \approx 1 - \left( \frac{3}{4\pi} \cdot \frac{(R_2^* - R_2)}{\gamma \cdot \Delta\chi_0 \cdot BVf \cdot Hct \cdot B_0} \right) \quad (2)$$

with  $\Delta\chi_0$  representing the susceptibility difference between deoxygenated and oxygenated red blood cells ( $\Delta\chi_0 = 0.264$  ppm at a magnetic field strength of  $B_0 = 9.4$  tesla).<sup>59</sup>  $StO_2$  is given in arbitrary units as magnetic field inhomogeneities  $B_0$  are not corrected. A haematocrit of  $Hct = 0.40$  can be used for the renal cortex and for the outer medulla (85%-95% of systemic Hct, which was assumed to be 0.45).<sup>60</sup>

Further to the equilibrium concentration regimen, renal blood volume can also be derived from dynamic susceptibility weighted imaging, where signal intensity changes in the kidney are monitored during the first passage of a ferumoxytol bolus as demonstrated in human studies.<sup>61</sup> This approach requires the measurement of the arterial concentration-signal-intensity-time-curve of ferumoxytol, designated as the arterial input function (AIF) and its deconvolution from the renal tissue signal intensity time curves. This technique is better suited for clinical applications than preclinical studies in small animals, where the small size of the relevant vessels makes the AIF measurement rather challenging.

## 5 | FERUMOXYTOL DOES NOT AFFECT REGULATION OF RENAL HAEMODYNAMICS AND OXYGENATION

Ferumoxytol is an approved intravascular iron supplementation therapy in the USA targeting patients with iron deficiency anaemia related to CKD. The preparation consists of USPIO nanoparticles encapsulated by a polyglucose sorbitol carboxymethylether coating. Ferumoxytol is superparamagnetic, which makes it a viable candidate as an off-label MRI contrast agent for a broad spectrum of preclinical and diagnostic imaging applications.<sup>44,45,62</sup> Ferumoxytol does not readily extravasate and is not filtered in the glomeruli, so it exhibits a long intravascular half-life of > 14 h in humans and about 2 h in small rodents. Ferumoxytol can be administered by intravenous injection.

A recent report studied acute intrinsic effects of ferumoxytol on the control of renal haemodynamics and oxygenation in rats.<sup>63</sup> This study was of high relevance as basic methodological principles require that a method intended to measure a certain variable per se does not alter this variable. For this purpose, *in vivo* measurements of arterial blood pressure, total renal blood flow (RBF, transsonic probe), local perfusion (laser-Doppler-flux) and tissue pO<sub>2</sub> (fluorescence quenching optodes) in the renal cortex and medulla of healthy rats were employed upon application of ferumoxytol.<sup>20,63,64</sup> Modulation of renal haemodynamics

and oxygenation was accomplished by dedicated test interventions.<sup>63</sup> The dose study included three (cumulative) doses of ferumoxytol: two low doses adapted from previous reports on monitoring the blood volume fraction of the brain and kidneys in rats, and a high-dose regimen that mimics the human equivalent dose (based upon body surface area) for the therapeutic application of ferumoxytol.<sup>63</sup> The main finding of these investigations in rats was that intravenously injected ferumoxytol has no sustained impact on renal haemodynamics and oxygenation under baseline physiological conditions as well as on control of haemodynamics and oxygenation as studied by hypoxic and hyperoxic stimuli and a brief suprarenal aortic occlusion (Figure 3).<sup>63</sup> The only significant finding reported was a moderate reduction in the hyperoxia-evoked increase in arterial pressure at a cumulative dose of 41 mg Fe/kg. This dose mimics the human equivalent dose for iron supplementation and is well beyond the dose commonly used for MR-based assessment of the renal BVf. The results demonstrated no immediate risk of impaired control of renal oxygenation or perfusion upon application of ferumoxytol. This observation rendered

ferumoxytol as an intravascular contrast medium suitable for the quantification and monitoring of changes in renal blood volume fraction.<sup>63</sup>

## 6 | MONITORING RENAL BVf DURING EXPERIMENTAL PHYSIOLOGICAL INTERVENTIONS

The applicability of ferumoxytol-enhanced MRI for probing renal BVf during physiological interventions that are concomitant with variations in BVf was recently demonstrated in healthy rats in conjunction with correcting renal  $T_2^*$  for BVf alterations.<sup>42</sup> For this purpose a dose finding study was performed first in rats to ensure that BOLD effects were detectable after ferumoxytol administration considering that the signal-to-noise ratio may be further diminished owing to  $T_2^*$  shortening attributed to the deoxygenation of blood.<sup>42</sup> Balancing the sensitivity of  $T_2^*$  to ferumoxytol injection and the  $T_2^*$  sensitivity to the (patho) physiological intervention (occlusion of the renal vein) a

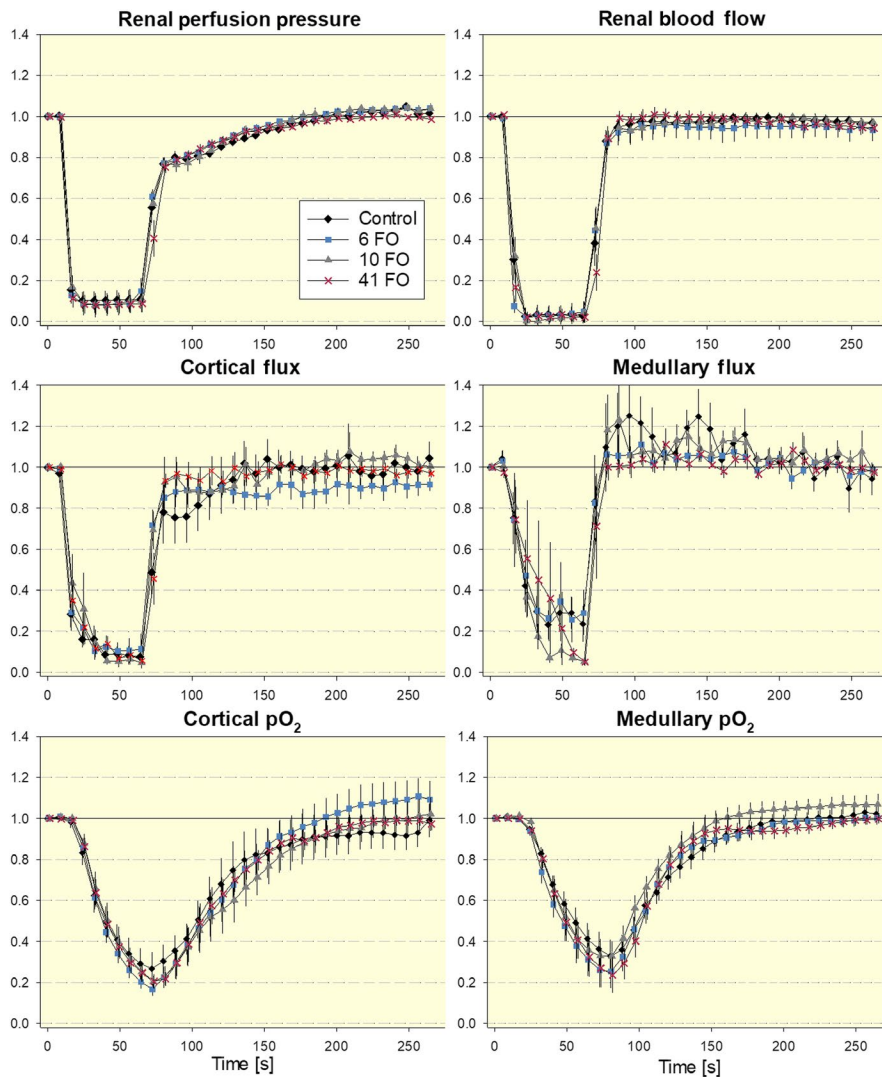


**FIGURE 3** Assessment of acute effects of ferumoxytol on the control of renal haemodynamics and oxygenation as studied by a brief occlusion of the suprarenal aorta and during recovery.<sup>63</sup> Ferumoxytol does not influence physiological changes during suprarenal aortic occlusion and recovery. Shown are relative changes in renal perfusion pressure, total renal blood flow (Transonic probe), cortical and medullary tissue perfusion (Flux, laser-Doppler-flux probes), and cortical and medullary tissue oxygen tension ( $pO_2$ , fluorescence-quenching probes) upon injection of isotonic saline (volume Control), and three consecutive injections of ferumoxytol to achieve cumulative doses of 6, 10 and 41 mg Fe/kg body mass (6 FO, 10 FO and 41 FO). Data are presented as mean  $\pm$  SEM

ferumoxytol dose of 2-4 mg Fe/kg BW was found to be best suited for  $R_2^*$ , BVf and  $StO_2$  mapping.  $\Delta R_2$  and  $\Delta R_2^*$  analyses revealed that BVf is higher in the outer medulla versus the renal cortex (Figure 4).<sup>42</sup>

Changes in the intrarenal BVf and  $StO_2$  were studied in rats in response to renal venous occlusion. Examples of renal cortical and outer medullary  $T_2^*$  maps are depicted in Figure 5. Renal BVf and  $StO_2$  maps obtained at baseline, during renal venous occlusion and during the recovery phase are illustrated in Figure 5. BVf and  $StO_2$  derived from MRI in rats were benchmarked against BVf and  $StO_2$  references provided by near infrared spectroscopy (NIRS) conducted in rats. The MRI data were in qualitative accordance with the NIRS data: cortical  $StO_2$  dropped substantially during the short-term venous occlusion for both approaches. The almost twofold increase in cortical BVf deduced from MRI during venous occlusion was in qualitative agreement with the rise in haemoglobin concentration per tissue volume derived from NIRS.

The main findings of the assessment of renal BVf during experimental physiological interventions in rats at 9.4 Tesla were fourfold<sup>42</sup>: (i) a 4 mg Fe/kg dose of ferumoxytol suits BVf assessment at 9.4 T during baseline, venous occlusion and recovery, (ii) the proposed approach permits reproducibility

for BVf and  $StO_2$  examination as validated by test/re-test experiments,<sup>42</sup> (iii) relative changes in cortical BVf and cortical  $StO_2$  derived from MRI were in qualitative accordance with relative changes in BVf and  $StO_2$  deduced from NIRS and (iv) without the monitoring of BVf MRI overestimates the  $StO_2$  decrease during renal venous occlusion.<sup>42</sup> To conclude, this experimental work permitted a non-invasive detection of renal BVf increase in rats upon venous occlusion and a removal of its effects on blood oxygenation-sensitized renal MR.

Probing renal BVf with ferumoxytol-enhanced MRI can be integrated with gold standard physiological measurements such as MR-PHYSIOL.<sup>37-39</sup> The insertion of invasive probes (combined  $pO_2$ - and laser-flux probes) into the kidney in the preclinical hybrid MR-PHYSIOL setting might induce a minor change in the intrarenal (tubular and blood) volume fractions. The volume of a kidney in the rats we usually study ranges between 1200  $\mu$ l and 1500  $\mu$ l. The combined volumes of two probes inserted (usually one into the cortex, one into the medulla) ranges between 30  $\mu$ l and 50  $\mu$ l. The amount of tissue (including the tubular and blood volume) “displaced” by two probes is about 2%-4%. This “volume shift” can be neglected for renal BVf assessment.

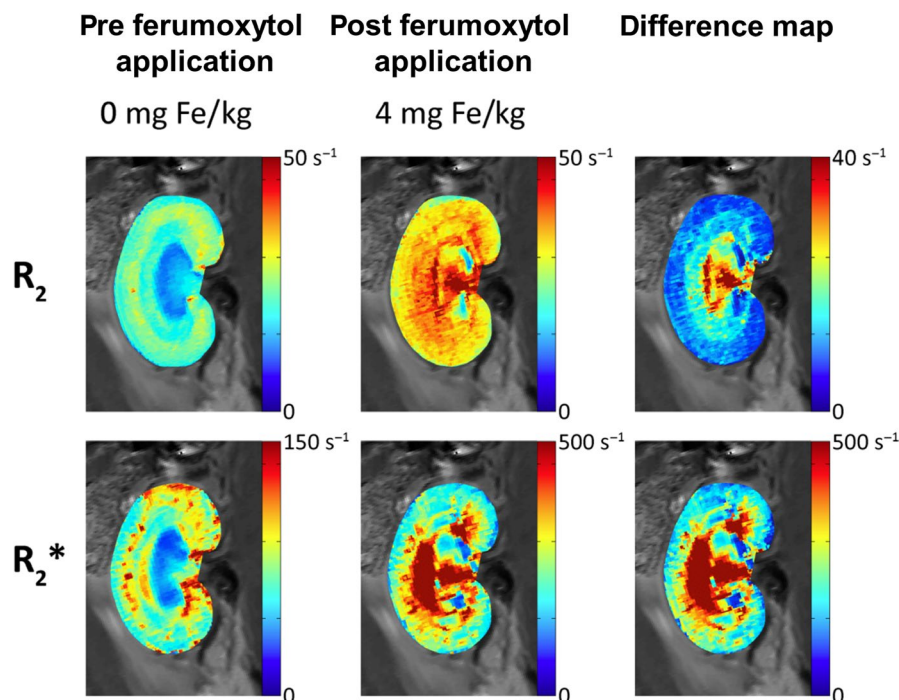


**FIGURE 4** Illustration of blood volume measurement procedure using ferumoxytol as an exogenous blood pool marker. Shown are parametric maps of renal  $R_2$  and  $R_2^*$  prior (left) to and after (middle) ferumoxytol administration.<sup>42</sup> Quantitative  $R_2$  and  $R_2^*$  maps permit comparisons over time and between animals, as they are not biased by external factors such as the RF coil sensitivity ( $B_1^-$ ) or the location of the subject with respect to the RF coil. The difference between  $R_2/R_2^*$  maps acquired before and after USPIO is closely related to the local BVf. The area with apparently very high BVf stretches from the papilla via the inner medulla to the central outer medulla. This phenomenon represents the influence of large iron-rich vessels located close to the image slice, rather than the actual medullary tissue properties. The locations of apparently high BVf in papilla and inner medulla co-localize with the renal artery and vein, and the interlobar arteries and veins

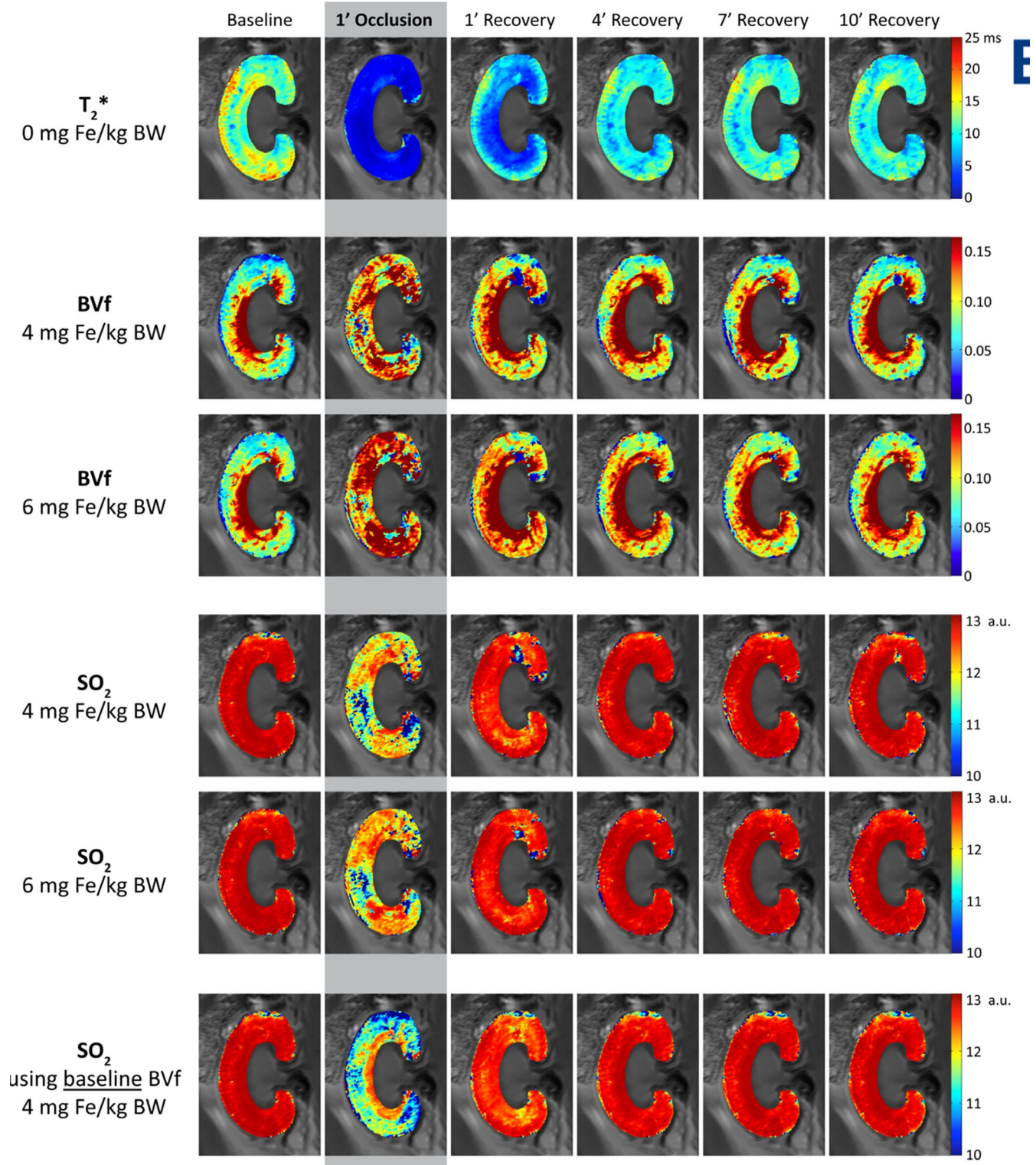


**FIGURE 5** Maps of renal cortical and outer medullary  $T_2^*$ , together with estimated maps of blood volume fraction (BVf) and oxygen saturation of Hb ( $SO_2$ ) at baseline, during renal venous occlusion and the recovery phase.<sup>42</sup> The maps at baseline and after 10 minutes of recovery are almost indistinguishable, confirming that the effects of venous occlusion were reversible. Within-subject repeatability is demonstrated for renal BVf and  $SO_2$  by comparing the maps derived from two different experimental phases, namely, following 4 mg Fe/kg USPIO and following 6 mg Fe/kg USPIO. Test-retest reliability (repeatability) was high—the differences between both iterations are nearly negligible, even though more USPIO had been injected in between. In addition,  $SO_2$  maps were calculated assuming that renal BVf remains constant and identical to the baseline condition (bottom row): the missing compensation for BVf changes during venous occlusion results in  $SO_2$  values considerably lower than when BVf was monitored

Notwithstanding these encouraging first results, benchmarking BVf and StO<sub>2</sub> results deduced from MRI against a quantitative reference is essential for further rigorous validation of the MRI approach. Currently, a perfect quantitative equivalent for validation of renal MR-derived BVf and StO<sub>2</sub> is not readily available. Invasive tissue pO<sub>2</sub> probes are very well established but cover very small renal regions. Another constraint is that invasive tissue pO<sub>2</sub> probes measure tissue pO<sub>2</sub> rather than blood oxygenation. NIRS affords estimation of StO<sub>2</sub> and tissue concentration of haemoglobin—an established surrogate for BVf—but the necessary mathematical modelling is rather complex and it is currently constrained to reflection mode probing of the renal cortex because of penetration depth limitations. However, benchmarking the occlusion-induced changes in cortical BVf and StO<sub>2</sub> derived from MRI with NIRS obtained for the renal cortex show good agreement. This observation provides encouragement for further advancement and integration of the MR approach into a comprehensive renal MR oximetry protocol.

## 7 | TOWARDS CLINICAL IMPLEMENTATION OF FERUMOXYTOL-ENHANCED MRI ASSESSMENT OF RENAL BVF

The R<sub>2</sub> and R<sub>2</sub>\* mapping protocols employed for renal BVf assessment in small rodents at ultrahigh magnetic field strengths are readily available on clinical MR scanners, which facilitates a swift translation into clinical use of ferumoxytol-based renal BVf examination. This development is fuelled by an ever-growing number of studies that report on the off-label use of ferumoxytol for a wide portfolio of preclinical and diagnostic imaging applications. In a clinical setting, renal T<sub>2</sub>\* and T<sub>2</sub> mapping is commonly employed at time points that are longitudinally propagated by at least hours if not days or months. With this clinical context, a temporal resolution of 2–3 min for combined T<sub>2</sub>\* and T<sub>2</sub> mapping and the 1–2 min time shift between the measurements of both parameters are negligible. MRI protocols affording breath-hold acquisitions facilitated by accelerated imaging using parallel acquisition techniques or compressed sensing approaches would make respiratory triggering obsolete, shorten examination times and enhance image quality by reducing the propensity to respiratory motion-induced image artefacts.

*En route* to clinical implementation ferumoxytol was demonstrated to be useful for differentiation between acute and chronic inflammatory kidney diseases based on different patterns of parenchymal ferumoxytol depositions in a rat model using a clinical whole-body 3.0 T MR scanner.<sup>65</sup> The sensitivity of ferumoxytol-enhanced R<sub>2</sub>\* mapping to dynamic BVf changes in the rat kidney was demonstrated using a 3.0 Tesla human MR scanner.<sup>66</sup>

Steady-state MR angiography using incremental doses of up to 4 mg/kg body weight of ferumoxytol as intravenous contrast agent was performed in patients with advanced kidney disease due for transplant listing, which implicitly supports the feasibility of renal BVf mapping in patients.<sup>67</sup> T<sub>2</sub>\* mapping has been also used to demonstrate that allografts undergoing acute rejection in paediatric kidney transplant patients show T<sub>2</sub>\* prolongation in ferumoxytol-enhanced MRI versus non-rejecting allografts.<sup>68</sup> This observation was attributed to reduced perfusion and increased oedema in rejecting allografts.<sup>68</sup> Normal R<sub>2</sub>\* values obtained for post-ferumoxytol administration (4 mg/kg body weight) at 1.5 T and 3.0 T were reported for the human kidney.<sup>69</sup> Pharmacokinetics of ferumoxytol in the kidney were examined in healthy subjects using R<sub>2</sub>\* relaxometry at 1.5 T and 3.0 T.<sup>70</sup> Renal R<sub>2</sub>\* increased at post-injection and peaked on day 1 (R<sub>2</sub>\*<sub>baseline</sub> = 13 s<sup>-1</sup> vs R<sub>2</sub>\*<sub>ferumoxytol</sub> = 31 s<sup>-1</sup>).<sup>70</sup> Clearance of ferumoxytol from the kidney occurred on day 2 for a ferumoxytol dose of 2mg/kg body weight. For a ferumoxytol dose of 4mg/kg body weight clearance from the kidney was reported on day 4 post-injection.<sup>70</sup> Renal T<sub>2</sub>\* decrease caused by ferumoxytol accumulation was demonstrated for healthy subjects and for type 1 diabetes patients.<sup>71</sup> A recent multicentre safety study enrolled 3215 patients who received 4240 ferumoxytol injections (dose range: 1–11 mg/kg body weight) for MRI.<sup>72</sup> The authors reported a positive safety profile for ferumoxytol use in MRI and concluded that diagnostic ferumoxytol was well tolerated and associated with no serious adverse events.<sup>72</sup> Ferumoxytol-enhanced dynamic MRI was employed in healthy subjects to assess the blood volume in the renal cortex (mean rBV<sub>renal cortex</sub> = 41±8 ml/100 g).<sup>61</sup> When implementing ferumoxytol-based renal BVf assessment in clinical renal imaging protocols, caution should be taken to prevent interference of ferumoxytol with other MRI techniques and MR contrasts. For example, ferumoxytol shortens the longitudinal relaxation time T<sub>1</sub>, which affects T<sub>1</sub> contrast.

Application of ferumoxytol might impact mapping of regional perfusion in renal tissue using arterial spin labelling (ASL) techniques.<sup>30,73–75</sup> The ASL technique employs magnetization-labelled water in arterial blood of the aorta or the renal arteries as a freely diffusible endogenous tracer. In a preparation module, spin labelling is applied to tag the longitudinal magnetization of arterial blood water before it enters the imaging plane in the kidney. An image covering the kidney is acquired following arterial blood labelling and a delay time between labelling and the advent of the tagged arterial blood water in the imaging plane. A control image is acquired of the same slice in the kidney using the same delay time but no labelling of the arterial blood water. Provided that the magnetization of the inflowing blood is the only difference between the control and the label image, a difference map yields a perfusion-weighted image of the kidney with the signal intensity being proportional to renal tissue perfusion.

$T_1$  shortening owing to the presence of ferumoxytol requires adaptation of the delay or traveling time used for arterial blood water in the arterial spin labelling preparation module. ASL approaches were exploited for examination of regional renal blood flow and were shown to be suitable for the evaluation of renal injury in rats<sup>76</sup> and for the assessment of patients suffering from diabetes and moderate (stage 3) CKD compared with healthy controls.<sup>30</sup> ASL MRI also provides an avenue towards MR-based assessment of arterial blood volume using multiple-delay time sampling as demonstrated for the human brain.<sup>77</sup> As ASL is a difference image technique and a low signal-to-noise ratio (SNR) technique, it might suffer from ferumoxytol-induced  $T_2^*$  shortening and SNR degradation. To decouple the interference of ferumoxytol with other MR techniques and MR contrasts, it is thus recommended that ferumoxytol-enhanced BVf assessments be performed at the end of clinical renal MRI protocols.

## 8 | FUTURE DIRECTIONS OF MAPPING RENAL BVF WITH MRI

Due caution for quantitative interpretation of renal BOLD-MRI is required as renal  $T_2^*$  is a surrogate that does not quantitatively reflect renal tissue oxygenation in several (patho) physiological conditions and because  $T_2^*$  may not mirror blood oxygenation quantitatively in some scenarios. This requires that renal blood oxygenation level-related  $T_2^*$  changes are strictly differentiated from  $T_2^*$  alterations caused by changes in tubular and vasculature volume fraction, the latter being  $T_2^*$  confounders.<sup>38</sup> To meet this goal, it is essential to incorporate an MR-based assessment of renal BVf into renal MRI protocols to detail vasodilation, vasoconstriction and other alterations in the blood volume fraction.<sup>24</sup>

It is well recognized that dynamic contrast-enhanced (DCE) methods in conjunction with tracer kinetic principles provide a viable alternative for the quantification of renal perfusion and blood volume.<sup>29,78-81</sup> For this purpose, bolus injection of exogenous contrast agents like gadolinium (Gd) chelates or iron oxide nanoparticles is administered.<sup>82-85</sup> Tracking and analysing the dynamic susceptibility contrast (DSC) changes during first-pass contrast agent bolus passage through the kidney requires fast imaging techniques with a temporal resolution of  $\leq 1$  s. It also requires the measurement of the arterial concentration-time-curve, designated as the arterial input function and its deconvolution from the time course of signal intensity in renal tissue. Renal DSC was successfully implemented in human studies and animal studies.<sup>80,82-85</sup> For the latter, methodological (imaging speed) and physiological (heart rate) constraints govern the achievable spatial resolution and render this approach particularly challenging in small rodents. Compartmental models used for the analysis of DCE signal intensity time course upon injection

of a gadolinium-based contrast bolus commonly include an extravascular component, leading to a complex mathematical kinetic description. Intravascularly confined contrast agents benefit DCE MRI as their kinetic models exclude the extravascular space. The experimental paramagnetic gadolinium-based contrast agent P792 is a rapid-clearance intravascularly confined agent characterized by negligible interstitial diffusion but unrestricted glomerular filtration.<sup>86-88</sup> This intravascular contrast agent has recently been evaluated for measurements of renal function in rats using a low dosage.<sup>89</sup>

Fluorine ( $^{19}\text{F}$ ) MRI offers an intriguing alternative to proton ( $^1\text{H}$ ) methods such as  $T_2^*$  and DCE imaging/mapping for quantifying changes in blood  $p\text{O}_2$  and blood volume in the kidney.  $^{19}\text{F}$  is another MR active nucleus with similar sensitivity to  $^1\text{H}$ . Although the absence of organic  $^{19}\text{F}$  in the body of humans and rodents is an advantage and any  $^{19}\text{F}$  compounds introduced in vivo can be detected with high selectivity and absolute specificity, its application is also challenged by typically low SNRs, especially when  $^{19}\text{F}$  compounds are administered systemically and distribute at low concentrations in vivo. Nonetheless, the application of fluorinated emulsions, typically prepared from perfluorocarbons (PFCs), has been explored to study vascular pathology in mice and rats<sup>90,91</sup> and recently, their utility to assess BVf and  $p\text{O}_2$  in the renal microvasculature was demonstrated following AKI in mice.<sup>92</sup>

Owing to the virtual absence of  $^{19}\text{F}$  in the human/animal body,  $^{19}\text{F}$  spin density-weighted MRI following intravenous injection of fluorinated emulsions may provide a quantitative measure of renal BVf. Compared with the USPIO-based approach, BVf assessment using  $^{19}\text{F}$  requires a reference with known concentration to be scanned together with the subject, and the much lower local concentration of  $^{19}\text{F}$  vs  $^1\text{H}$  requires measures to counteract the SNR challenge, such as increasing signal averaging and/or lowering spatial resolution. To this end, in the context of renal MR oximetry, conceptually it is more appealing to exploit directly the blood oxygenation sensitivity of PFC (as outlined in the following), rather than using it for probing BVf to correct for effects of BVf variations from  $T_2^*$ -based blood oxygenation measurements.

PFC emulsions have a high oxygen-dissolving capacity making them ideal  $\text{O}_2$  carriers as well as indicators of  $p\text{O}_2$  changes. The longitudinal relaxation rate ( $1/T_1$ ) of  $^{19}\text{F}$  in PFCs was shown to depend linearly on  $\text{O}_2$  partial pressure.<sup>93</sup> This led to the first non-invasive in vivo tissue  $\text{O}_2$  assessments in tumour tissue and liver in mice<sup>94</sup> and later in the myocardial tissue of rats.<sup>95</sup> The latter study provided the first proof-of-concept study for rapid, non-invasive measurements of  $\text{O}_2$  tension changes in response to ischaemia and reperfusion using  $^{19}\text{F}$  MRI.<sup>95</sup> More recently, a decreased renal BVf and blood  $p\text{O}_2$  was detected in the cortico-medullary junction 24 h following unilateral renal ischaemia reperfusion using  $^{19}\text{F}$  MRI, and in parallel an increased  $T_2^*$

was observed by  $^1\text{H}$  BOLD MRI.<sup>92</sup> In the injured kidney, the  $T_2^*$ ,  $^{19}\text{F}$  signal and  $\text{pO}_2$  within the renal cortex were comparable with the contralateral non-injured kidney, but in the inner medulla, vascular leakage and extravascular retention of PFC NPs resulted in reduced  $T_2^*$ , increased  $^{19}\text{F}$  and unchanged  $\text{pO}_2$ . These results suggest a recovery in perfusion and oxygenation within the cortex but not within the inner medulla.<sup>92</sup> This study shows the potential of applying PFC emulsions for studying renal disease. The relatively large size of the nanoparticles within these emulsions ( $> 100$  nm) might provide a relatively good safety profile with respect to renal toxicity, as they are not expected to be cleared through glomerular filtration. Therefore, unlike other imaging agents that undergo renal clearance (eg iodinated x-ray contrast agents, gadolinium-based MR contrast agents), PFC emulsions are not immediately considered as nephrotoxic, thereby holding promise for in vivo tissue  $\text{pO}_2$  assessment of renal tissue in animal models of AKI.<sup>92</sup>

One of the most exciting areas of innovation in biomedical imaging concerns the visualization on multiple scales in space and time: imaging biological objects in size ranging from the atomic to the anatomic scale, and from nanoseconds to decades in large population imaging studies.<sup>96</sup> Advances in biomedical imaging have spurred developments and applications in the fields of optical, high-frequency ultra-sound and photoacoustic imaging.<sup>97</sup> The progress in photoacoustic imaging provides a trajectory into the characterization of (patho)physiological conditions of the kidney, which could allow early detection of kidney injury owing to its capacity to probe renal oxygen saturation of haemoglobin.<sup>98</sup> This development underlines the potential and value of hybrid and complementary modalities in basic research and clinical science, such as optoacoustic imaging and MRI, photoacoustic imaging and intravital 2-photon microscopy or near infrared spectroscopy (NIRS) and MRI,<sup>40</sup> and their calibration with quantitative gold standards.<sup>96</sup>

## 9 | CONCLUSION

We should definitely not skip BOLD for renal imaging. What we need to do is to re-evaluate our understanding of BOLD imaging as validated bio- or imaging marker for renal tissue oxygenation. For this, we (only) need to decipher and quantify the changes in the vascular and tubulus volume fraction that are confounding BOLD imaging. This calibration will empower BOLD imaging and its application in the research setting and in the clinical arena. It can be expected that there are several (patho)physiological conditions in which the knowledge of BVf will not be as essential (eg in early stage diabetes) as for other more complex scenarios (eg in kidney transplantation). These considerations are necessary to make valid statements about renal blood oxygenation, especially

in cases where BVf is not significantly different from the normal healthy physiological condition. It still remains to be determined whether errors introduced by ignoring BVf in specific settings remain within acceptable error margins or not.

To conclude, further weight should be put behind the solution of the remaining issues to advance the (pre)clinical value and the capabilities of parametric MRI for probing dynamic changes in the renal blood volume with the goal to decipher the confounding impact of the vascular compartment on  $T_2^*$  en route to improving our understanding of haemodynamics/oxygenation in kidney disorders. A swift transfer of MR oximetry, including  $T_2^*$  mapping and renal BVf quantification, from the research scenario into the clinic should be targeted in interdisciplinary and interinstitutional collaboration networks among forward-thinking basic researchers, application scientists and clinicians to establish a comprehensive MR protocol for the in vivo and non-invasive assessment of renal haemodynamics and oxygenation. As this approach may become increasingly used in (pre)clinical research, it should help to enhance the potential of MRI for the assessment of renal diseases.

## ACKNOWLEDGEMENTS

This work was funded in part (T. Niendorf, E. Seeliger, A. Pohlmann and S. Waiczies) by the German Research Foundation (Gefördert durch die Deutsche Forschungsgemeinschaft (DFG), Projektnummer 394046635, SFB 1365, RENOPROTECTION). Funded by the Deutsche Forschungsgemeinschaft (DFG, German Research Foundation), Project number 394046635, SFB 1365, RENOPROTECTION and in part (T. Niendorf and E. Seeliger) by the German Federal Ministry of Research and Education (renalMRoxy, program VIP+, 03VP00081).

## CONFLICT OF INTEREST

The authors have no conflict of interest to declare.

## ORCID

Thoralf Niendorf  <https://orcid.org/0000-0001-7584-6527>

Sonia Waiczies  <https://orcid.org/0000-0002-9916-9572>

Andreas Pohlmann  <https://orcid.org/0000-0002-8572-2568>

## REFERENCES

1. Kramer H. Kidney disease and the westernization and industrialization of food. *Am J Kidney Dis.* 2017;70(1):111-121.
2. Camara NO, Iseki K, Kramer H, Liu ZH, Sharma K. Kidney disease and obesity: epidemiology, mechanisms and treatment. *Nat Rev Nephrol.* 2017;13(3):181-190.
3. Levin A, Tonelli M, Bonventre J, et al. Global kidney health 2017 and beyond: a roadmap for closing gaps in care, research, and policy. *Lancet.* 2017;390(10105):1888-1917.
4. Bello AK, Levin A, Tonelli M, et al. Assessment of global kidney health care status. *JAMA.* 2017;317(18):1864-1881.

5. Eckardt KU, Coresh J, Devuyst O, et al. Evolving importance of kidney disease: from subspecialty to global health burden. *Lancet*. 2013;382(9887):158-169.
6. Persson PB. Renoprotection. *Acta Physiol*. 2017;219(3):540-541.
7. Matejovic M, Ince C, Chawla LS, et al. Renal hemodynamics in AKI: In search of new treatment targets. *Journal of the American Society of Nephrology: JASN*. 2016;27(1):49-58.
8. Fortrie G, de Geus HRH, Betjes MGH. The aftermath of acute kidney injury: a narrative review of long-term mortality and renal function. *Crit Care*. 2019;23(1):24.
9. Grenier N, Merville P, Combe C. Radiologic imaging of the renal parenchyma structure and function. *Nat Rev Nephrol*. 2016;12(6):348-359.
10. Wang Y, Bellomo R. Cardiac surgery-associated acute kidney injury: risk factors, pathophysiology and treatment. *Nat Rev Nephrol*. 2017;13(11):697-711.
11. Evans RG, Ince C, Joles JA, et al. Haemodynamic influences on kidney oxygenation: The clinical implications of integrative physiology. *Clin Exp PharmacolPhysiol*. 2013;40:106-122.
12. Seeliger E, Sendeski M, Rihal CS, Persson PB. Contrast-induced kidney injury: mechanisms, risk factors, and prevention. *Eur Heart J*. 2012;33(16):2007-2015.
13. Gomez H, Ince C, De BD, et al. A unified theory of sepsis-induced acute kidney injury: inflammation, microcirculatory dysfunction, bioenergetics, and the tubular cell adaptation to injury. *Shock*. 2014;41(1):3-11.
14. Ow CPC, Ngo JP, Ullah MM, Hilliard LM, Evans RG. Renal hypoxia in kidney disease: Cause or consequence? *Acta Physiol (Oxf)*. 2018;222(4):e12999.
15. Chawla LS, Eggers PW, Star RA, Kimmel PL. Acute kidney injury and chronic kidney disease as interconnected syndromes. *N Engl J Med*. 2014;371(1):58-66.
16. Nangaku M, Rosenberger C, Heyman SN, Eckardt KU. Regulation of hypoxia-inducible factor in kidney disease. *Clin Exp Pharmacol Physiol*. 2013;40(2):148-157.
17. Evans RG, Lankadeva YR, Cochrane AD, et al. Renal haemodynamics and oxygenation during and after cardiac surgery and cardiopulmonary bypass. *Acta Physiol (Oxf)*. 2018;222(3):10.
18. Evans RG, Ow CP, Bie P. The chronic hypoxia hypothesis: the search for the smoking gun goes on. *Am J Physiol Renal Physiol*. 2015;308(2):F101-F102.
19. Hoff U, Lukitsch I, Chaykovska L, et al. Inhibition of 20-HETE synthesis and action protects the kidney from ischemia/reperfusion injury. *Kidney Int*. 2011;79(1):57-65.
20. Seeliger E, Cantow K, Arakelyan K, Ladwig M, Persson PB, Flemming B. Low-dose nitrite alleviates early effects of an X-ray contrast medium on renal hemodynamics and oxygenation in rats. *Invest Radiol*. 2014;49(2):70-77.
21. Seeliger E, Flemming B, Wronski T, et al. Viscosity of contrast media perturbs renal hemodynamics. *J Am Soc Nephrol*. 2007;18(11):2912-2920.
22. Calzavacca P, Evans RG, Bailey M, Bellomo R, May CN. Cortical and medullary tissue perfusion and oxygenation in experimental septic acute kidney injury. *Crit Care Med*. 2015;43(10):e431-e439.
23. Cantow K, Flemming B, Ladwig-Wiegard M, Persson PB, Seeliger E. Low dose nitrite improves reoxygenation following renal ischemia in rats. *Sci Rep*. 2017;7(1):14597-15058.
24. Niendorf T, Pohlmann A, Arakelyan K, et al. How bold is blood oxygenation level-dependent (BOLD) magnetic resonance imaging of the kidney? Opportunities, challenges and future directions. *Acta Physiol (Oxf)*. 2015;213(1):19-38.
25. Zhang B, Wang Y, Wang C, et al. Comparison of blood oxygen level-dependent imaging and diffusion-weighted imaging in early diagnosis of acute kidney injury in animal models. *J Magn Reson Imaging*. 2019;50(3):719-724.
26. Hoff U, Bubalo G, Fechner M, et al. A synthetic epoxyeicosatrienoic acid analogue prevents the initiation of ischemic acute kidney injury. *Acta Physiol (Oxf)*. 2020;227(2):e13297.
27. Pohlmann A, Hentschel J, Fechner M, et al. High temporal resolution parametric MRI monitoring of the initial ischemia/reperfusion phase in experimental acute kidney injury. *PLoS ONE*. 2013;8(2):e57411.
28. Vakilzadeh N, Zanchi A, Milani B, et al. Acute hyperglycemia increases renal tissue oxygenation as measured by BOLD-MRI in healthy overweight volunteers. *Diabetes Res Clin Pract*. 2019;150:138-143.
29. Pruijm M, Mendichovszky IA, Liss P, et al. Renal blood oxygenation level-dependent magnetic resonance imaging to measure renal tissue oxygenation: a statement paper and systematic review. *Nephrol Dial Transplant*. 2018;33 (suppl 2):ii22-ii28.
30. Prasad PV, Li LP, Thacker JM, et al. Cortical perfusion and tubular function as evaluated by magnetic resonance imaging correlates with annual loss in renal function in moderate chronic kidney disease. *Am J Nephrol*. 2019;49(2):114-124.
31. Haddock B, Larsson HBW, Francis S, Andersen UB. Human renal response to furosemide: Simultaneous oxygenation and perfusion measurements in cortex and medulla. *Acta Physiol (Oxf)*. 2019;227(1):e13292.
32. Mendichovszky I, Pullens P, Dekkers I, et al. Technical recommendations for clinical translation of renal MRI: a consensus project of the Cooperation in Science and Technology Action PARENCHIMA. *MAGMA*. 2019.
33. Ogawa S, Lee TM, Kay AR, Tank DW. Brain magnetic resonance imaging with contrast dependent on blood oxygenation. *Proc Natl Acad Sci USA*. 1990;87(24):9868-9872.
34. Ogawa S. Finding the BOLD effect in brain images. *NeuroImage*. 2012;62(2):608-609.
35. Pruijm M, Milani B, Burnier M. Blood oxygenation level-dependent MRI to assess renal oxygenation in renal diseases: progresses and challenges. *Front Physiol*. 2016;7:667.
36. Pedersen M, Dissing TH, Morkenborg J, et al. Validation of quantitative BOLD MRI measurements in kidney: application to unilateral ureteral obstruction. *Kidney Int*. 2005;67(6):2305-2312.
37. Cantow K, Arakelyan K, Seeliger E, Niendorf T, Pohlmann A. Assessment of renal hemodynamics and oxygenation by simultaneous magnetic resonance imaging (MRI) and quantitative invasive physiological measurements. *Methods Mol Biol*. 2016;1397:129-154.
38. Pohlmann A, Arakelyan K, Hentschel J, et al. Detailing the Relation Between Renal T2\* and Renal Tissue pO2 Using an Integrated Approach of Parametric Magnetic Resonance Imaging and Invasive Physiological Measurements. *Invest Radiol*. 2014;49(8):547-560.
39. Pohlmann A, Cantow K, Hentschel J, et al. Linking non-invasive parametric MRI with invasive physiological measurements (MR-PHYSIOL): towards a hybrid and integrated approach for investigation of acute kidney injury in rats. *Acta Physiol (Oxf)*. 2013;207(4):673-689.
40. Grosenick D, Cantow K, Arakelyan K, et al. Detailing renal hemodynamics and oxygenation in rats by a combined near-infrared

- spectroscopy and invasive probe approach. *Biomedical optics express*. 2015;6(2):309-323.
41. Niendorf T, Flemming B, Evans RG, Seeliger E. What Do BOLD MR imaging changes in donors' remaining kidneys tell us? *Radiology*. 2016;281(2):653-655.
  42. Pohlmann A, Cantow K, Huelnhagen T, et al. Experimental MRI monitoring of renal blood volume fraction variations en route to renal magnetic resonance oximetry. *Tomography*. 2017;3(4):188-200.
  43. Storey P, Ji L, Li LP, Prasad PV. Sensitivity of USPIO-enhanced R2 imaging to dynamic blood volume changes in the rat kidney. *J Magn Reson Imaging*. 2011;33(5):1091-1099.
  44. Bashir MR, Bhatti L, Marin D, Nelson RC. Emerging applications for ferumoxytol as a contrast agent in MRI. *J Magn Reson Imaging*. 2015;41(4):884-898.
  45. Vasanawala SS, Nguyen KL, Hope MD, et al. Safety and technique of ferumoxytol administration for MRI. *Magn Reson Med*. 2016;75(5):2107-2111.
  46. Rivera-Rivera LA, Johnson KM, Turski PA, Wieben O, Schubert T. Measurement of microvascular cerebral blood volume changes over the cardiac cycle with ferumoxytol-enhanced T2 (\*) MRI. *Magn Reson Med*. 2019;81(6):3588-3598.
  47. Toth GB, Varallyay CG, Horvath A, et al. Current and potential imaging applications of ferumoxytol for magnetic resonance imaging. *Kidney Int*. 2017;92(1):47-66.
  48. Persson PB. Good publication practice in physiology 2017: Current Revisions of the Recommendations for the Conduct, Reporting, Editing and Publication of Scholarly Work in Medical Journals. *Acta Physiol (Oxf)*. 2017;221(4):283-284.
  49. Persson PB. Good publication practice in physiology 2019. *Acta Physiol (Oxf)*. 2019;227(4):e13405.
  50. Evans RG, Gardiner BS, Smith DW, O'Connor PM. Methods for studying the physiology of kidney oxygenation. *Clin Exp Pharmacol Physiol*. 2008;35(12):1405-1412.
  51. Brown RW, Cheng YCN, Haacke EM, Thompson MR, Venkatesan R *Magnetic Resonance Imaging: Physical Principles and Sequence Design 2nd*, edition edn. Hoboken, New Jersey, USA: Wiley Blackwell; 2014.
  52. Niendorf T, Pohlmann A, Reimann HM, et al. Advancing cardiovascular, neurovascular, and renal magnetic resonance imaging in small rodents using cryogenic radiofrequency coil technology. *Frontiers in pharmacology*. 2015;6:255.
  53. Tropres I, Lamalle L, Peoc'h M, et al. In vivo assessment of tumoral angiogenesis. *Magn Reson Med*. 2004;51(3):533-541.
  54. Kim T, Hendrich KS, Masamoto K, Kim SG. Arterial versus total blood volume changes during neural activity-induced cerebral blood flow change: implication for BOLD fMRI. *J Cereb Blood Flow Metab*. 2007;27(6):1235-1247.
  55. Wang F, Jiang RT, Tantawy MN, et al. Repeatability and sensitivity of high resolution blood volume mapping in mouse kidney disease. *J Magn Reson Imaging*. 2014;39(4):866-871.
  56. Christen T, Lemasson B, Pannetier N, et al. Evaluation of a quantitative blood oxygenation level-dependent (qBOLD) approach to map local blood oxygen saturation. *NMR Biomed*. 2011; 24(4):393-403.
  57. He X, Yablonskiy DA. Quantitative BOLD: mapping of human cerebral deoxygenated blood volume and oxygen extraction fraction: default state. *Magn Reson Med*. 2007;57(1):115-126.
  58. Yablonskiy DA, Haacke EM. Theory of NMR signal behavior in magnetically inhomogeneous tissues: the static dephasing regime. *Magn Reson Med*. 1994;32(6):749-763.
  59. Spees WM, Yablonskiy DA, Oswood MC, Ackerman JJ. Water proton MR properties of human blood at 1.5 Tesla: magnetic susceptibility, T(1), T(2), T\*(2), and non-Lorentzian signal behavior. *Magn Reson Med*. 2001;45(4):533-542.
  60. Rasmussen SN. Intrarenal red cell and plasma volumes in the non-diuretic rat. Determination by means of 51Cr labelled red cells and 125I-gamma-M-immunoglobulin. *Pflugers Arch*. 1973; 342(1):61-72.
  61. Morell A, Ahlstrom H, Schoenberg SO, Abildgaard A, Bock M, Bjornerud A. Quantitative renal cortical perfusion in human subjects with magnetic resonance imaging using iron-oxide nanoparticles: influence of T1 shortening. *Acta Radiol*. 2008;49(8):955-962.
  62. Hope MD, Hope TA, Zhu C, et al. Vascular imaging with ferumoxytol as a contrast agent. *AJR Am J Roentgenol*. 2015; 205(3):W366-373.
  63. Cantow K, Pohlmann A, Flemming B, et al. Acute effects of ferumoxytol on regulation of renal hemodynamics and oxygenation. *Sci Rep*. 2016;6:29965.
  64. Arakelyan K, Cantow K, Hentschel J, et al. Early effects of an x-ray contrast medium on renal T(2) \*/T(2) MRI as compared to short-term hyperoxia, hypoxia and aortic occlusion in rats. *Acta Physiol (Oxf)*. 2013;208(2):202-213.
  65. Budjan J, Neudecker S, Schock-Kusch D, et al. Can ferumoxytol be used as a contrast agent to differentiate between acute and chronic inflammatory kidney disease? feasibility study in a rat model. *Invest Radiol*. 2016;51:100-105.
  66. Storey P, Ji L, Li L-P, Prasad PV. Sensitivity of USPIO-enhanced R(2) imaging to dynamic blood volume changes in the rat kidney. *Journal of magnetic resonance imaging : JMRI*. 2011; 33:1091-1099.
  67. Stoumpos S, Hennessy M, Vesey AT, et al. Ferumoxytol-enhanced magnetic resonance angiography for the assessment of potential kidney transplant recipients. *Eur Radiol*. 2018;28(1):115-123.
  68. Aghighi M, Pisani L, Theruvath AJ, et al. Ferumoxytol Is Not Retained in Kidney Allografts in Patients Undergoing Acute Rejection. *Molecular imaging and biology : MIB : the official publication of the Academy of Molecular Imaging*. 2018;20(1):139-149.
  69. Stirrat CG, Alam SR, MacGillivray TJ, et al. Ferumoxytol-enhanced magnetic resonance imaging methodology and normal values at 1.5 and 3T. *Journal of cardiovascular magnetic resonance: official journal of the Society for Cardiovascular Magnetic Resonance*. 2016;18(1):46.
  70. Wells SA, Schubert T, Motosugi U, et al. Pharmacokinetics of Ferumoxytol in the Abdomen and Pelvis: A Dosing Study with 1.5- and 3.0-T MRI Relaxometry. *Radiology*. 2019;190489.
  71. Kordbacheh H, Baliyan V, Parakh A, Wojtkiewicz GR, Hedgire S, Harisinghani MG. Pictorial review on abdominal applications of ferumoxytol in MR imaging. *Abdom Radiol (NY)*. 2019;44(10):3273-3284.
  72. Nguyen KL, Yoshida T, Kathuria-Prakash N, et al. Multicenter safety and practice for off-label diagnostic use of ferumoxytol in MRI. *Radiology*. 2019;190477.
  73. Odudu A, Nery F, Hartevelde AA, et al. Arterial spin labelling MRI to measure renal perfusion: a systematic review and statement paper. *Nephrol Dial Transplant*. 2018;33(suppl 2):ii15-ii21.
  74. Wang J, Zhang Y, Yang X, et al. Hemodynamic effects of furosemide on renal perfusion as evaluated by ASL-MRI. *Acad Radiol*. 2012;19(10):1194-1200.

75. Zhang JL, Lee VS. Renal perfusion imaging by MRI. *J Magn Reson Imaging*. 2019. <https://doi.org/10.1002/jmri.26911> [Epub ahead of print].
76. Liu YP, Song R, Liang C, Chen X, Liu B. Arterial spin labeling blood flow magnetic resonance imaging for evaluation of renal injury. *Am J Physiol Renal Physiol*. 2012;303(4):F551-558.
77. Yoshiura T, Hiwatashi A, Yamashita K, et al. Simultaneous measurement of arterial transit time, arterial blood volume, and cerebral blood flow using arterial spin-labeling in patients with Alzheimer disease. *AJNR Am J Neuroradiol*. 2009;30(7):1388-1393.
78. Buchanan CE, Mahmoud H, Cox EF, et al. Quantitative assessment of renal structural and functional changes in chronic kidney disease using multi-parametric magnetic resonance imaging. *Nephrol Dial Transplant*. 2019. <https://doi.org/10.1093/ndt/gfz129> [Epub ahead of print].
79. Selby NM, Blankestijn PJ, Boor P, et al. Magnetic resonance imaging biomarkers for chronic kidney disease: a position paper from the European Cooperation in Science and Technology Action PARENCHIMA. *Nephrol Dial Transplant*. 2018;33(suppl 2);ii4-ii14.
80. Caroli A, Pruijm M, Burnier M, Selby NM. Functional magnetic resonance imaging of the kidneys: where do we stand? The perspective of the European COST Action PARENCHIMA. *Nephrol Dial Transplant*. 2018;33(suppl 2);ii1-ii3.
81. Zhang JL, Rusinek H, Chandarana H, Lee VS. Functional MRI of the kidneys. *J Magn Reson Imaging*. 2013;37(2):282-293.
82. Schoenberg SO, Aumann S, Just A, et al. Quantification of renal perfusion abnormalities using an intravascular contrast agent (part 2): results in animals and humans with renal artery stenosis. *Magn Reson Med*. 2003;49(2):288-298.
83. Aumann S, Schoenberg SO, Just A, et al. Quantification of renal perfusion using an intravascular contrast agent (part 1): results in a canine model. *Magn Reson Med*. 2003;49(2):276-287.
84. Zimmer F, Zollner FG, Hoeger S, et al. Quantitative renal perfusion measurements in a rat model of acute kidney injury at 3T: testing inter- and intramethodical significance of ASL and DCE-MRI. *PLoS ONE*. 2013;8(1):e53849.
85. Pedersen M, Laustsen C, Perot V, Basseau F, Moonen C, Grenier N. Renal hemodynamics and oxygenation in transient renal artery occluded rats evaluated with iron-oxide particles and oxygenation-sensitive imaging. *Z Med Phys*. 2010;20(2):134-142.
86. Port M, Corot C, Raynal I, et al. Physicochemical and biological evaluation of P792, a rapid-clearance blood-pool agent for magnetic resonance imaging. *Invest Radiol*. 2001;36(8):445-454.
87. Port M, Corot C, Rousseaux O, et al. P792: a rapid clearance blood pool agent for magnetic resonance imaging: preliminary results. *MAGMA*. 2001;12(2-3):121-127.
88. Gaillard S, Kubiak C, Stolz C, Bonnemain B, Chassard D. Safety and pharmacokinetics of p792, a new blood-pool agent: results of clinical testing in nonpatient volunteers. *Invest Radiol*. 2002;37(4):161-166.
89. Mandry D, Pedersen M, Odille F, et al. Renal functional contrast-enhanced magnetic resonance imaging: evaluation of a new rapid-clearance blood pool agent (p792) in sprague-dawley rats. *Invest Radiol*. 2005;40(5):295-305.
90. Dardzinski BJ, Sotak CH. Rapid tissue oxygen tension mapping using 19F inversion-recovery echo-planar imaging of perfluoro-15-crown-5-ether. *Magn Reson Med*. 1994;32(1):88-97.
91. Noth U, Morrissey SP, Deichmann R, et al. In vivo measurement of partial oxygen pressure in large vessels and in the reticuloendothelial system using fast 19F-MRI. *Magn Reson Med*. 1995;34(5):738-745.
92. Hu L, Chen J, Yang X, et al. Assessing intrarenal nonperfusion and vascular leakage in acute kidney injury with multinuclear (1) H/ (19) F MRI and perfluorocarbon nanoparticles. *Magn Reson Med*. 2014;71(6):2186-2196.
93. Parhami P, Fung BM. Fluorine-19 relaxation study of perfluorochemicals as oxygen carriers. *J Phys Chem*. 1983;87(11):4.
94. Mason RP, Nunnally RL, Antich, PP. Tissue oxygenation: a novel determination using 19F surface coil NMR spectroscopy of sequestered perfluorocarbon emulsion. *Magn Reson Med*. 1991;18(1):71-79.
95. Mason RP, Jeffrey FM, Malloy CR, Babcock EE, Antich PP. A noninvasive assessment of myocardial oxygen tension: 19F NMR spectroscopy of sequestered perfluorocarbon emulsion. *Magn Reson Med*. 1992;27(2):310-317.
96. Niendorf T, Frydman L, Neeman M, Seeliger E. Google maps for tissues: multiscale imaging of biological systems and disease. *Acta Physiol (Oxf)*. 2020;228(2):e13392.
97. Gerling M, Zhao Y, Nania S, et al. Real-time assessment of tissue hypoxia in vivo with combined photoacoustics and high-frequency ultrasound. *Theranostics*. 2014;4(6):604-613.
98. Okumura K, Matsumoto J, Iwata Y, et al. Evaluation of renal oxygen saturation using photoacoustic imaging for the early prediction of chronic renal function in a model of ischemia-induced acute kidney injury. *PLoS ONE*. 2018;13(12):e0206461.

**How to cite this article:** Niendorf T, Seeliger E, Cantow K, Flemming B, Waiczies S, Pohlmann A. Probing renal blood volume with magnetic resonance imaging. *Acta Physiol*. 2020;228:e13435. <https://doi.org/10.1111/apha.13435>